Title

Characterization of groove density variation of VLS gratings with ALS XROL LTP-II in different operation modes

ISBN

978-1-5106-3790-0

Authors

Lacey, Ian

Yashchuk, Valeriy V

Publication Date

2020-08-21

DOI

10.1117/12.2568705

Peer reviewed

Characterization of groove density variation of VLS gratings with ALS XROL LTP-II in different operation modes

Ian Lacey*[a] and Valeriy V. Yashchuk[a]
[a]Lawrence Berkeley National Laboratory, 1 Cyclotron Rd., Berkeley, California 94720

ABSTRACT

The long trace profiler, LTP-II, available at the Advanced Light Source (ALS) X-ray Optics Laboratory (XROL), was recently upgraded by replacing a multimode diode laser light source with a single-mode, wavelength-stabilized, fiber-coupled diode laser system. The upgrade enables us to reliably characterize the lateral variation of groove density of variable-line-spacing (VLS) x-ray diffraction gratings. Here, we discuss the LTP-II performance with an example of measurements with a VLS grating with the groove density at the grating center of 300 lines/mm. For the measurements, we use the LTP-II in two different operation arrangements, the single Gaussian beam and the pencil beam interferometer arrangements. For each operation arrangement, we apply two data processing algorithms: with calculating the centroid position and with determining the position of a characteristic features of the detected beam intensity distributions. We discuss the observed strong correlation between the LTP-II modes of operation and the resulted (extracted) groove density variations. We also speculate on possible origin of the correlation.

Keywords: x-rays, slope metrology, long trace profiler, LTP, diffraction measurements, x-ray grating, variable-line-spacing, VLS grating

1. INTRODUCTION

The long trace profiler, LTP-II [1], available at the Advanced Light Source (ALS) X-ray Optics Laboratory (XROL) [2], was recently upgraded by replacing a multimode diode laser light source with a single-mode, wavelength-stabilized, fiber-coupled diode laser system [3]. The upgrade has enabled us to reliably characterize the lateral variation of groove density of variable-line-spacing (VLS) x-ray diffraction gratings in the manner discussed, for example, in Refs. [4-6].

After the upgrade, the LTP-II was used [7] to measure the groove density distribution of the VLS double-grating (1000 and 2000 lines/mm) fabricated for the ALS AMBER beamline 6.0.1 spectrometer [8]. Due to the high variation of grove density specified for that AMBER grating, the range of the diffraction angle in visual-light first-order Littrow-configuration diffraction exceeded the angular dynamic range of the LTP (± 5 mrad) by a factor of ~7. As a result, the spatial range of a single scan run was limited to 12 mm, whereas the length of the grating clear aperture was 80 mm. This forced us to search for a method for stitching multiple overlapping traces in the tangential direction. In Ref. [7], we have suggested an experimental method, which can make such stitching measurements possible. The method utilizes the strong dependence of the diffracted beam intensity distribution in the LTP focal plane on peculiarities of the grating surface profile, experimentally observed with the AMBER grating. Matching of the intensity distributions measured at the points of the overlapped areas of the shifted traces can allow precise stitching of the traces. This work is in progress.

For realization of the approach suggested in Ref. [7], we need to overcome the problem of measurement perturbation related to the LTP-II systematic errors, including those due to carriage wobbling (see also discussion in Ref. [9]). The straightforward solution of this problem is to use the LTP-II as a sensor in a profiler based on deflectometry with a movable pentaprism. This is the arrangement suggested and realized in the LTP available at the SOLEIL [5]. Unfortunately, the movable pentaprism arrangement is currently unavailable with the XROL LTP-II.

In this paper, we discuss the LTP-II measurements with a VLS grating fabricated for the LCLS by diamond ruling. With the grating, we have performed a series of measurements to validate the performance of the LTP-II for characterization of groove-density distribution of such gratings in the different operation modes. The paper is organized as following: The design and specification of the VLS grating under test, as well as the measurement approach are briefly discussed in Sec. 2. Section 3 provides the details of the experimental arrangement and procedure for the XROL LTP-II measurements with the VLS gratings. The results of the measurements are discussed in Sec. 4. The major observation is

*ilacey@lbl.gov; phone 1 510 486-4117; als.lbl.gov

the strong dependence of the measured grove density distribution on the mode of operation of the LTP-II. The paper concludes (Sec. 5) by summarizing the main concepts discussed through the paper and outlining a plan for future work.

2. LCLS GRATING SPECIFICATION AND THE DYNAMIC ANGULAR RANGE OF THE MEASUREMENTS

Figure 1 presents the image and dimensional sketch of the LCLS grating under discussion.

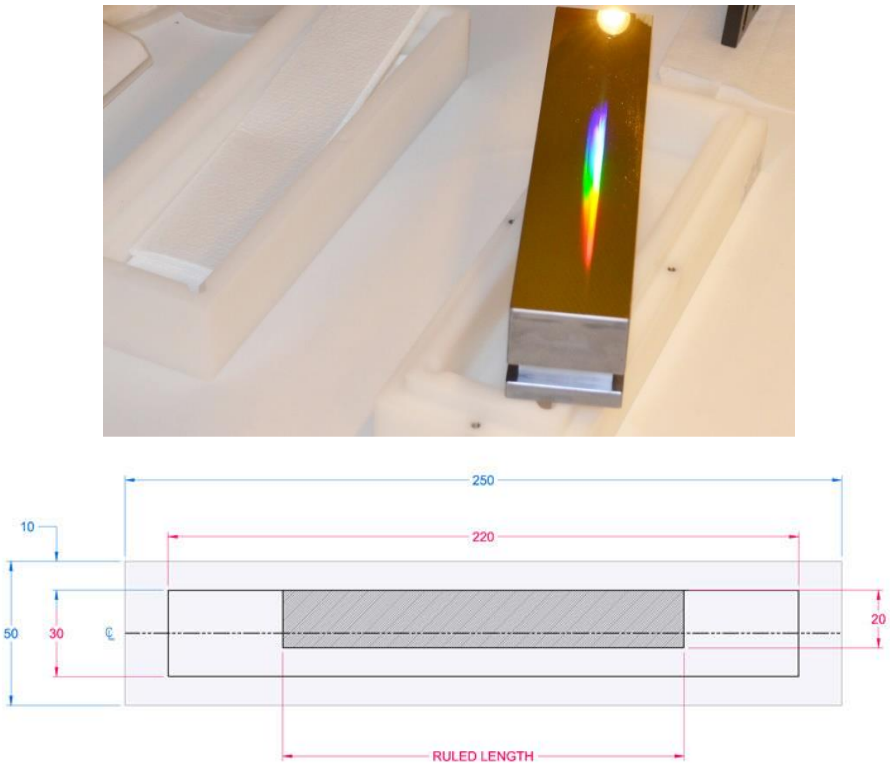

Figure 1: The image and the dimensional sketch of the LCLS VLS grating discussed in the present paper (courtesy Daniele Cocco). The total length of the ruled area measured here is ±110 mm.

The specification (in terms of coefficients of the desired polynomial function) of the grating groove density distribution are summarized in Table 1.

Table 1: Specification of the LCLS grating groove density distribution.

Parameter	Specification
g_0 (l/mm)	300.0
g_1 (l/mm^2)	-0.0252
g_2 (l/mm^3)	0
g_3 (l/mm^4)	0

The LTP-II measurements with the grating were performed in the Littrow configuration, when the directions of the incidence and diffraction beams in the selected order coincide for the grating center. Let us start from the diffraction equation for a grating with varying groove density:

$$\sin\alpha_0 - \sin\left[\beta_0 + \delta\beta_m(x_i)\right] = m\lambda g(x_i)\,, \tag{1}$$

where α_0 is the angle of incidence, calculated from the surface normal and positive at the counterclockwise direction (Fig. 2), β_0 is the diffraction angle at the grating center (calculated from the surface normal and positive at the clockwise direction), $x = 0$, $\delta\beta_m(x_i)$ is the variation of the diffraction angle for the *m*-th order, λ is the wavelength of the probe beam light, $g(x_i)$ is the groove density distribution in the tangential point with coordinate x_i. With the sign convection in Eq. (1), in the perfect Littrow configuration, $\beta_0 = -\alpha_0$.

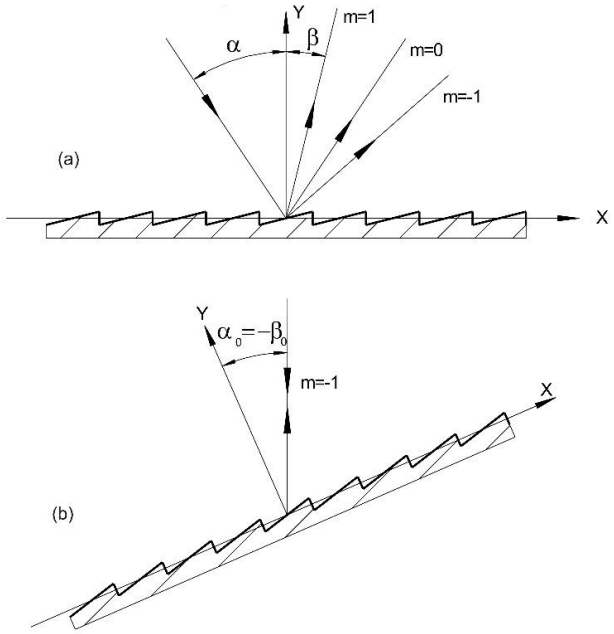

Figure 2: (a) Convention on the incidence and diffraction angles as defined in Eq. (1). Here the both angles α and β are positive. (b) The Littrow configuration arrangement for $m = -1$ order diffractions, corresponding to the LTP-II measurements with the LCLS grating (see Sec. 3). In the plot (b), the diffraction angle is positive and the incidence angle is negative: $\alpha_0 = -\beta_0$.

We should remember that the LTP-II is calibrated for measurements of surface slope variation of mirrors. Therefore, in the LTP calibration, the doubling of the light-beam deflection angle due to the surface slope is accounted with a factor of ½. Correspondingly, to get the value of $\delta\beta_m(x_i)$, the LTP-II reading in the sample channel, $\gamma(x_i)$, has to be multiplied by a factor of 2. Additionally, we should account for the sign difference of the diffraction angle as defined in Eq. (1) and the surface slope angle as measured with the LTP. Indeed, the positive surface slope angle leads to reflection of the light beam in the counterclockwise direction – see Fig. 2. The direction of increase of the diffraction angle is opposite and corresponds to decrease of the groove density of a VLS grating. Therefore, $\delta\beta_m(x_i) = -2 \cdot \gamma(x_i)$.

At $g(x_i = 0) = 300$ lines/mm and $\lambda = 632.875$ nm, corresponding to the LTP-II light source (see Fig. 3), the minus first order ($m = -1$) Littrow angle is rather small, $\alpha_0 \approx -5.45$ degrees. Therefore, a reliable measurement in the first order diffraction can be performed with the grating tilted by α_0 with respect to the horizontal face-up alignment (Fig. 4), used for characterization of the grating surface slope variation in the zero order. Unfortunately, currently we haven't the capability for precise monitoring (measurement) of the grating tilt angle when the Littrow configuration is desired (see also discussion in Sec. 3, below).

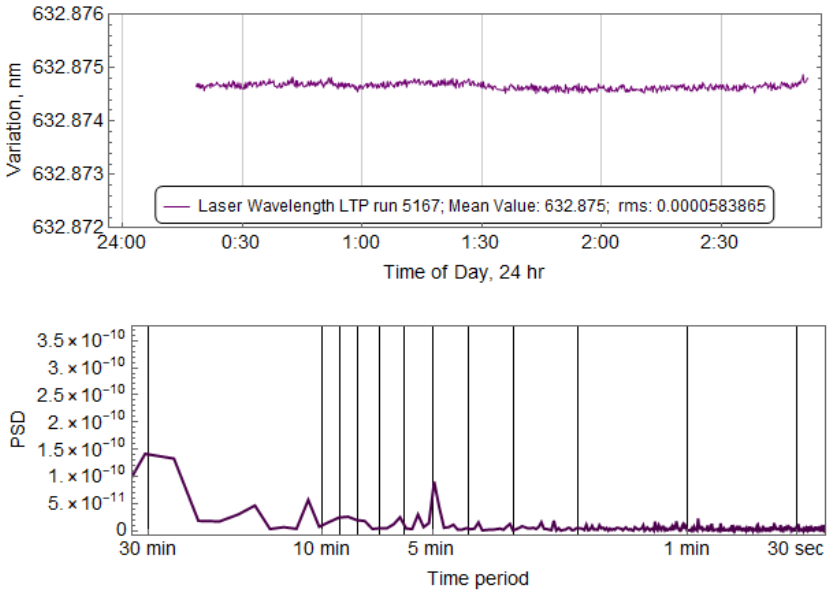

Figure 3: (a) Temporal variation of wavelength of the light from the new LTP-II diode-laser light source as recorded during the first scan of a 4-scan run of a diffraction angle measurement with the LCLS grating and (b) the corresponding power spectral density. In the course of the LTP measurements, the wavelength is continuously monitored with a Bristol Instruments' wavelength meter of 671B-VIS model.

By defining the groove density variation $\delta g(x_i)$ as [$g_0 \equiv g(x=0)$]

$$\delta g(x_i) = g(x_i) - g_0 , \tag{2}$$

Eq. (1) can be reduced to the form of relation between the variation of the diffraction angle $\delta\beta_m(x_i)$ and the variation of the groove density, $\delta g(x_i)$:

$$\begin{aligned} &\sin\alpha_0 - \sin\left[\beta_0 + \delta\beta_m(x_i)\right] = m\lambda\left(g_0 + \delta g(x_i)\right), \quad \text{or} \\ &\sin\beta_0 - \sin\left[\beta_0 + \delta\beta_m(x_i)\right] = m\lambda\cdot\delta g(x_i). \end{aligned} \tag{3}$$

From Eq. (3), for the linear groove density variation, specified in Table 1 for the grating under test with the tangential size of the grating aperture of ±110 mm, the total variation of the first-order diffraction angle (for the Littrow configuration) is ∓ 1.763 mrad; well within the angular dynamic range of the XROL LTP-II.

Equation (3) does not account for the substrate's surface slope variation and the errors of the measurements, such as the change of the incidence angle due to the LTP carriage wobbling when scanning. We consider the contributions of these perturbations to the measurements with VLS gratings in the next section.

3. EXPERIMENTAL ARRANGEMENT AND PROCEDURE FOR MEASUREEMTNS

Figure 4 shows the LTP-II experimental arrangement, used for characterization of groove density variation of the LCLS grating.

The two arrangements, shown in Fig. 4, correspond to the grating under test aligned for the measurements in the zero order [image (a)] and in the first order [image (b)] diffraction in the Littrow configuration. The corresponding readings of an electronic level, placed on the kinematic stage together with the grating, are –0.4 degrees (due to a tilt of the sample beam of the current LTP-II optical sensor from the vertical direction) and +5.0 degrees.

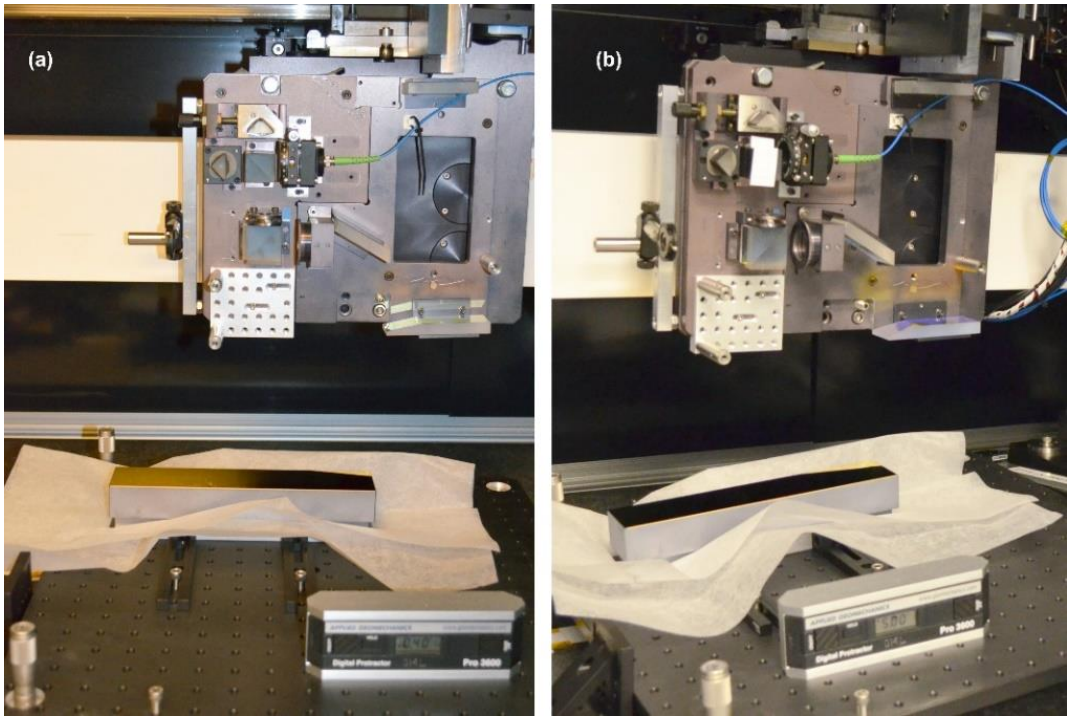

Figure 4: Experimental arrangement of the LTP-II with the VLS grating aligned for the measurements (a) in the zero order and (b) in the first order diffraction in the Littrow configuration. The corresponding readings of the electronic level, placed on the kinematic stage together with the grating, are -0.4 degrees (due to a tilt of the sample beam of the current LTP-II optical sensor) and +5.0 degrees.

Two series of measurements were carried out with the LTP in two different modes of operation. First, we used the single-Gaussian beam (SGB) mode with the second beam blocked by a paper stopper placed inside the beam splitter system of the LTP optical sensor (Fig. 4b). Second, we used the LTP in the classical pencil-beam-interferometer (PBI) mode. In this case, the stopper was removed (Fig. 4a). We have recently demonstrated that the LTP spatial resolution of surface slope measurements in these two modes is significantly different [10]. Additionally, these modes of operation can have different sensitivity to the LTP-II systematic errors [3,11]. Therefore, it is interesting to understand the effect of the different resolution on the groove measurements with the LTP in the SGB and PBI modes of operation.

With the scanning LTP optical head, the wobbling of the carriage is a principal source of the systematic error of the measurements. In the LTP-II, the wobbling angle is recorded in the reference arm as a function of the carriage position, $\omega(x_i)$.

In order to account for the wobbling angle, it should be added to Eq. (3) as a variation of α_0; similarly, we account for the surface slope error, $s(x_i)$:

$$\begin{aligned} &\sin[\alpha_0 + err(x_i)] - \sin\left[\beta_0 + \delta\beta_m(x_i)\right] = m\lambda\left(g_0 + \delta g(x_i)\right), \quad \text{or} \\ &\sin[\alpha_0 + err(x_i)] - \sin\alpha_0 + \sin\beta_0 - \sin\left[\beta_0 + \delta\beta_m(x_i)\right] = m\lambda \cdot \delta g(x_i), \end{aligned} \tag{4}$$

where, the error trace is defined as

$$err(x_i) = w(x_i) - s(x_i) \tag{5}$$

with mutually opposite sign of $s(x_i)$ and $\omega(x_i)$ terms, corresponding to their contribution to the effective incidence angle $\alpha(x_i) \equiv \alpha_0 + err(x_i)$, counted from the surface normal to the counterclockwise direction in a particular position x_i.

Let us first confirm the sign of the surface slope error contribution to the incidence angle, defined in Eqs. (4) and (5). Assuming that the local surface slope error is positive, then the local normal to the surface is rotated counterclockwise (refer to Fig. 2b). Therefore, the effective incidence angle is decreased.

Next, let us check the sign of the contribution to α_0 of the wobbling error. We know that in the current arrangement of the LTP-II (without a Dove prism) [12], in order to correctly account the wobbling error in the surface slope measurements, we should add the wobbling error, measured in the LTP-II reference channel, to the slope trace measured in the sample channel. If the measured wobbling angle is positive, then the carriage is effectively rotated counterclockwise, and the effective incidence angle increases.

In the course of groove-density measurements with the LTP-II, the wobbling error is routinely measured in the LTP-II reference channel – Fig. 5.

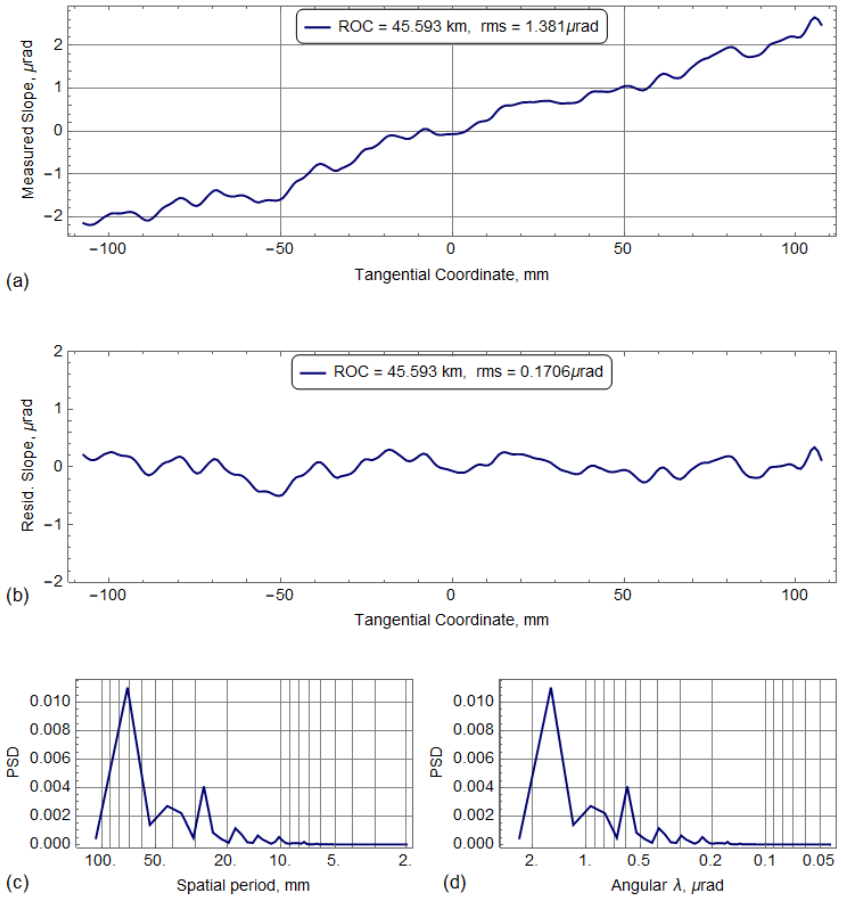

Figure 5: (a) Slope variation due to the carriage wobbling, as recorded in the LTP-II reference channel, (b) the residual (after subtraction of the best-fit linear variation) wobbling error, and (c) the PSD distribution of the residual slope trace in the plot (b). The peak-to-valley (PV) and root-mean-square (RMS) variations of the reference slope trace are 4.6 μrad and 0.17 μrad (after subtraction of the linear trend), correspondingly. The random noise of ~ 0.2 μrad (RMS), associated with the air convection along the optical path of the LTP-II reference beam, has been Gaussian filtered with a radius of 4 points.

The wobbling angle trace in Fig. 5 is the result of averaging over 4 sequential scans of a single measurement run, arranged according the scanning strategy, optimal for suppression of the instrumental drift errors described with second-order polynomial function [13].

Because of the long optical path in the LTP-II reference arm, the wobbling angle measurements suffer from the large random noise due to air convection along the optical path. In order to suppress the contribution of the noise to the result, we apply to the recorded reference data Gaussian filtering with a radius of 4 points. This procedure has been thoroughly verified in the measurements with the XROL Optical Surface Measuring System (OSMS) [14,15]].

In order to obtain the data on the surface slope error of the grating substrate, we perform additional measurements in the zero-order arrangement – Fig. 6. The surface slope error trace in Fig. 6 is also the result of averaging over 4 optimally arranged [13] sequential scans of a single measurement run.

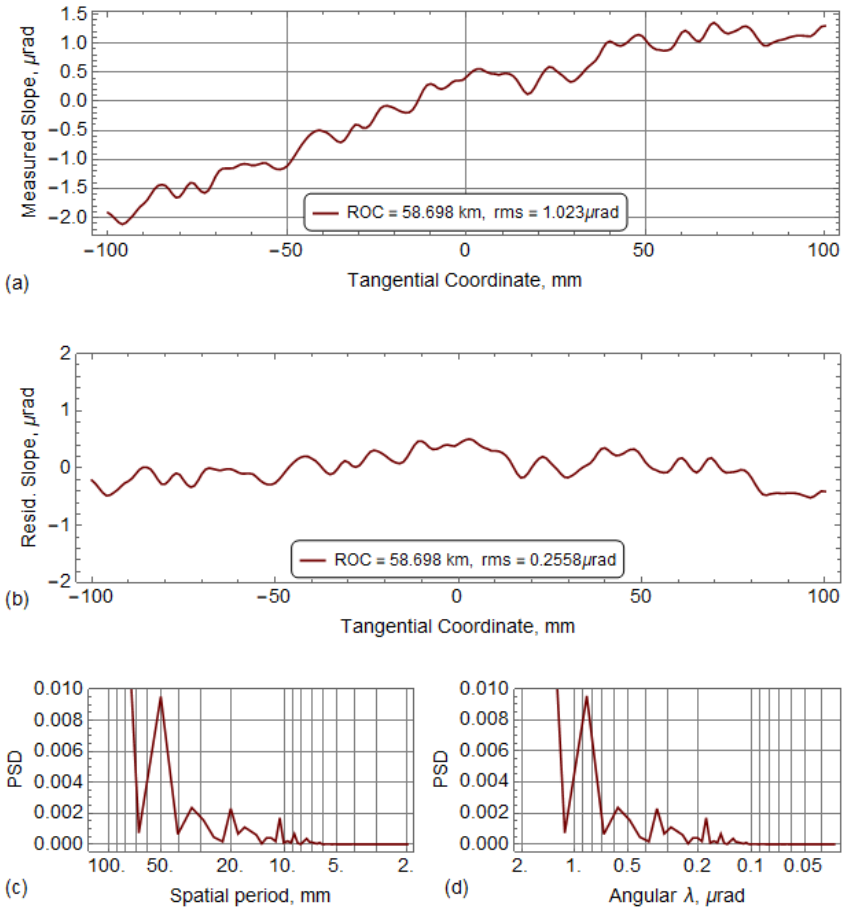

Figure 6: The grating substrate surface slope variation (a) as recorded by the LTP-II in the SGB mode with the grating in the zero order diffraction, and (b) after subtraction of the best-fit cylindrical shape with radius of curvature of 56.7 km. The peak-to-valley (PV) and root-mean-square (RMS) residual slope variations are ~3.5 μrad and 0.25 μrad (after subtraction of the linear trend), correspondingly. The corresponding PSD spectra of the surface slope variation in terms of spatial period (c) and angular period (d).

The good news for the current measurements with the VLS grating under test is that in the resulted error term, $err(x_i)$, the contributions due to the carriage wobbling and the surface slope error compensate each other (see Fig. 7).

At first glance, the approximate mutual compensation of the errors due to the LTP-II carriage wobbling and the surface imperfection of the grating substrate make the error term $err(x_i)$ in Eq. (4) practically unimportant, so it can be ignored.

Unfortunately, the situation is not so easy. In LTP measurements of the grating groove density, the incidence and diffraction angles are coupled through a transcendental equation (4), rather than linearly coupled, as in the case of measurements with reflective optics. Therefore, the correct averaging of a series of scans should be performed in the grove density domain. This means that first, Eq. (4) has to be applied to each scan to calculate the grove density variation for this scan and, second, the obtained traces of the grove density variation are averaged for the final result.

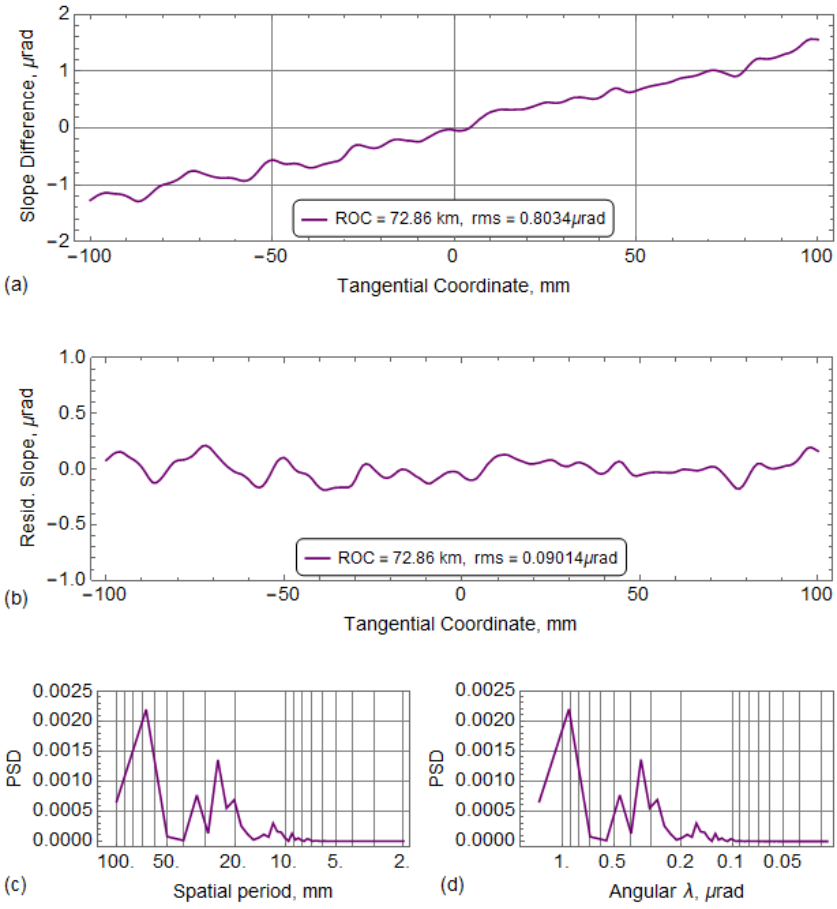

Figure 7: The error term calculated as the difference of the carriage wobbling error and the grating substrate surface slope variation. The peak-to-valley (PV) and root-mean-square (RMS) of the error term are ±1.4 μrad and 0.09 μrad, correspondingly.

There is another problem with reliable extraction of the groove density variation $\delta g(x_i)$ from the measured variation of the diffraction angle $\delta\beta_m(x_i)$. Besides the nonlinear dependence on measurement errors, as discussed above, the precisice conversion of $\delta\beta_m(x_i)$ to $\delta g(x_i)$ requires high accuracy values of the initial incidence and diffraction angles, α_0 and β_0.

As mentioned in Sec. 2, in the current LTP-II arrangement (Fig. 3), we cannot accurately measure α_0 and β_0. We even cannot be sure that when we align the grating for measurements in the Littrow configuration (as we think), β_0 is exactly equal to $-\alpha_0$. This is also because of the 0.4-degree tilt of the grating, needed for the zero-order measurements (see Fig. 4a).

Note that the zero-order angular tilt of the sample beam in the current LTP-II is unavoidable because the first priority alignment of the laser beam is to direct the reference beam perfectly along the axis of the carriage translation. After this alignment, the sample beam is left as is. The assembly the current LTP optical sensor with the fixed (glued) optical elements has an artificial rotation of the beam splitters introduced for suppression of unwanted interferences of the light back-reflected in these optical elements (see discussion in other contribution to this conference [16]).

In collaboration with the "father" of the PBI-based LTP profilers, Dr. Peter Takacs, we are currently working on the LTP-II upgrade. One of the major goals of the upgrade is to develop a slope profiler capable for precision measurements with VLS diffraction gratings. In this profiler, we plan to use our precision rotation stage, ARFA [17], in order to enable the accurate measurements of the Littrow configuration angles.

Given the uncertainty in the values of α_0 and β_0 to be probably larger than $err(x_i)$ and assuming that the error term does not significantly vary from scan to scan (see Sec. 4), we omit it when fitting the data obtained with the LCLS grating. Without the error term in Eq. (4), the diffraction angle variation depends solely on the initial diffraction angle:

$$\sin\left[\beta_0 + \delta\beta_{-1}(x_i)\right] - \sin\beta_0 = \lambda \cdot \delta g(x_i), \tag{6}$$

where we have accounted for $m = -1$ in the current measurements with the LCLS grating placed in the minus-first-order Littrow configuration.

In order to convert the LTP-II measurements of the variation of the diffraction angle $\delta\beta_m(x_i)$ to the variation of the groove density $\delta g(x_i)$, we use

$$\beta_0 = -\alpha_0 = 0.0950743\,\text{rad} \tag{7}$$

that corresponds to a 'normalization' of the result to the desired (specified) groove density in the position of the grating center. The value of the Littrow configuration angle in Eq. (7) is calculated using $g(x_i = 0) = 300$ lines/mm and the measured value of the sample-beam-light wavelength of $\lambda = 0.000632874$ mm (see Sec. 2).

Note that when we apply Eq. (6) to extract the value of $\delta g(x_i)$ in a particular position x_i, we are using the value of the light wavelength measured for the same point:

$$\delta g(x_i) = \frac{1}{\lambda(x_i)}\left(\sin\left[\beta_0 + \delta\beta_{-1}(x_i)\right] - \sin\beta_0\right), \tag{8}$$

measured with the wavelength meter (Fig. 3).

4. THE RESULTS OF THE LTP-II MEASUREMENTS WITH THE LCLS GRATING

Figure 8 shows the groove density distributions resulted from the diffraction angle measurements with the LTP-II in the SGB mode of operation when the centroid calculation positioning (CCP) is used for evaluation of the measured angle.

Figure 9 presents the results of reprocessing of the same measurements with the LTP-II in the SGB mode of operation, as in Fig. 8, but with evaluation of the measured diffraction angle from the position of the maximum of the best-fit Gaussian function that is the Gaussian maximum fitting (GMF) algorithm.

The residual, after subtraction of the best-fit linear trend (as specified), distributions are shown. The corresponding values of the linear coefficient are inset in the plots.

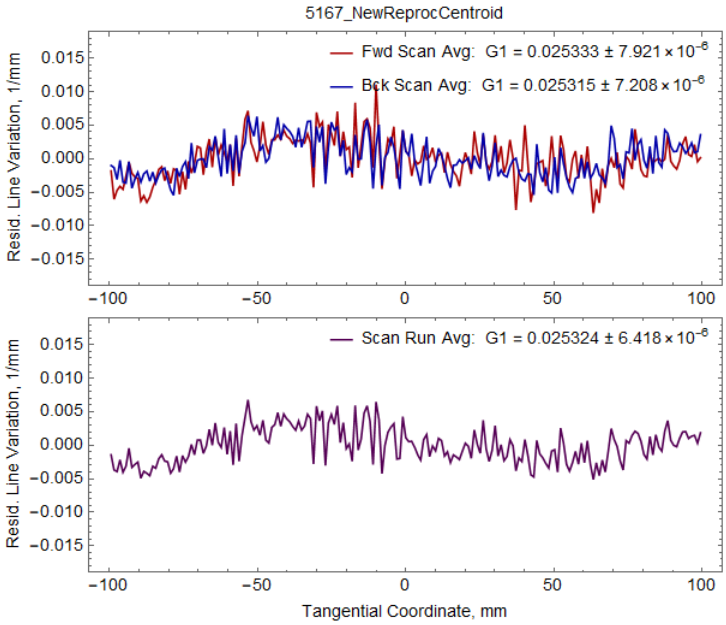

Figure 8: Groove density distributions as calculated from the diffraction angle measurements with the LTP-II in the SGB mode of operation using CCP algorithm for evaluation of the measured angle: (the top plot) the groove density distributions measured with the LTP-II scanning in the forward direction (the red line) and in the backward direction (the blue line), and (the bottom plot) the groove density distribution averaged over all 4 measurements, performed according to the optimal scanning strategy FBBF [13]. The residual, after subtraction of the best-fit linear trend (as specified), distributions are shown. The corresponding values of the linear coefficient are inset in the plots.

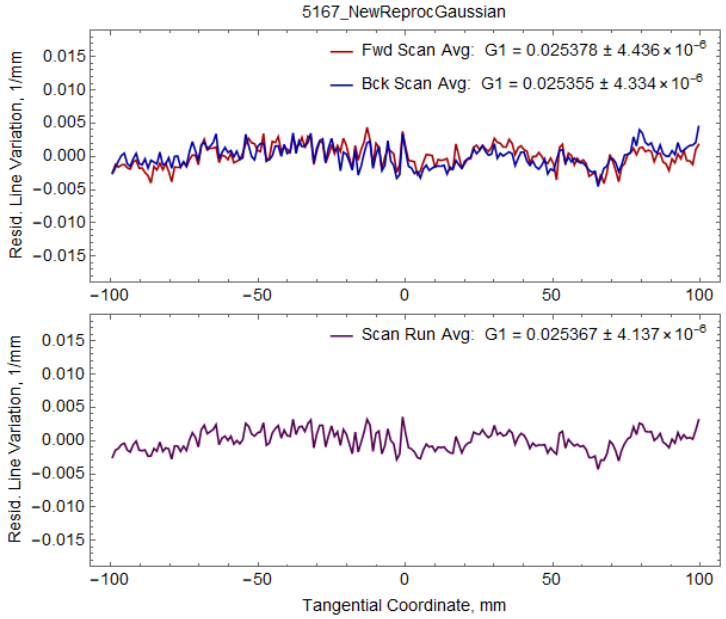

Figure 9: Groove density distributions as calculated from the diffraction angle measurements with the LTP-II in the SGB mode of operation using GMF algorithm: (the top plot) the groove density distributions measured with the LTP-II scanning in the forward direction (the red line) and in the backward direction (the blue line), and (the bottom plot) the groove density distribution averaged over all 4 measurements, performed according to the optimal scanning strategy FBBF [13]. The residual, after subtraction of the best-fit linear trend (as specified), distributions are shown.

Figures 10 and 11 present the results of measurements with the LTP-II in the PBI mode of operation, obtained with two different algorithms of data processing, with centroid calculation positioning (Fig. 10) and with second-order-polynomial fitting, SOPF (Fig. 11).

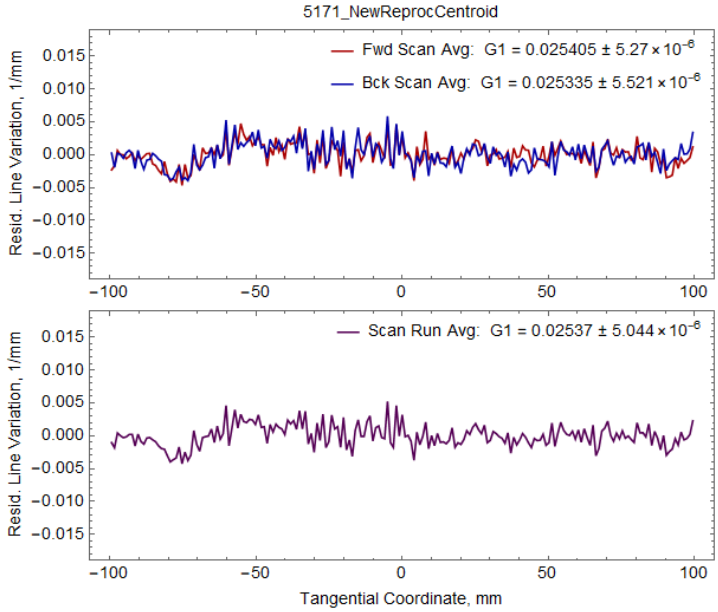

Figure 10: Groove density distributions as calculated from the diffraction angle measurements with the LTP-II in the PBI mode of operation using CCP algorithm for evaluation of the measured angle: (the top plot) the groove density distributions measured with the LTP-II scanning in the forward direction (the red line) and in the backward direction (the blue line), and (the bottom plot) the groove density distribution averaged over all 4 measurements, performed according to the optimal scanning strategy FBBF [13]. The residual, after subtraction of the best-fit linear trend (as specified), distributions are shown. The corresponding values of the linear coefficient are inset in the plots.

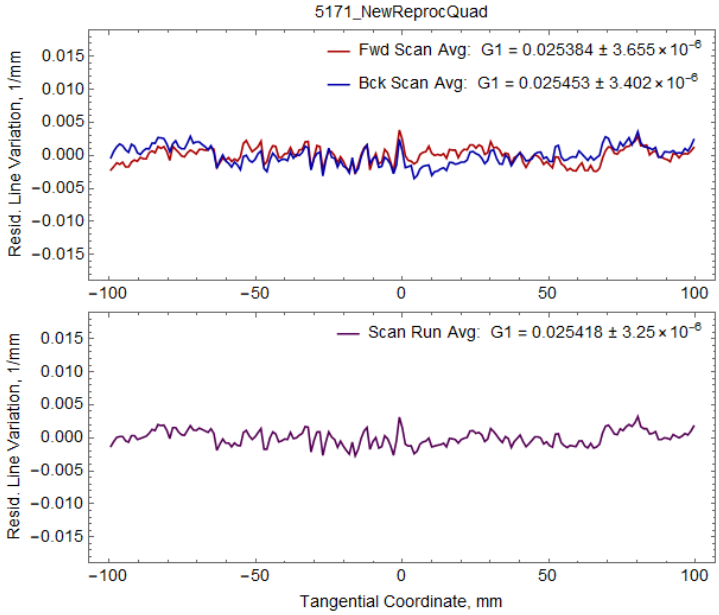

Figure 11: Groove density distributions as calculated from the diffraction angle measurements with the LTP-II in the PBI mode of operation using SOPF algorithm: (the top plot) the groove density distributions measured with the LTP-II scanning in the forward direction (the red line) and in the backward direction (the blue line), and (the bottom plot) the groove density distribution averaged over all 4 measurements, performed according to the optimal scanning strategy FBBF [13]. The residual, after subtraction of the best-fit linear trend (as specified), distributions are shown.

In Figs. 8-11, the residual, after subtraction of the best-fit linear trend (as specified), distributions are shown as extracted from the measurements, performed in the forward and backward direction (the top plot). The bottom plot presents the resulted distribution, averaged over 4 scans, performed according to the optimal scanning strategy FBBF [13].

The major observation from the results of the LTP-II measurements with the LCLS VLS grating shown in Figs. 8-11, is the strong correlation of the residual groove density variation with the LTP-II mode of operation and data processing. The smaller variation corresponds to the operation modes with lower spatial resolution, the SGB/GMF and PBI/SOPF, correspondingly (compere with the results of the resolution measurement in Ref. [10]).

However, the difference of different modes in the effective lateral resolution can hardly explain the observed significant difference of the low-spatial-frequency variations of the groove density distributions, extracted from the same measurement data, but processed with different algorithms. We can speculate that the observed difference may also relate to a difference in the systematic error and spatial resolution of the LTP-II in the different operation/data processing modes [3] (see also discussion in Ref. [11]).

In Figs. 9-11, the residual, after subtraction of the best-fit linear trend (as specified), distributions of the groove density are shown together with the corresponding values of the best-fit linear coefficient, corresponding to the grating parameter g_1. These results are summarized in Table 2, together with the statistical error of the fitting.

Table 2: The coefficient of the linear variation of the groove density distribution of the VLS grating under test, measured at the XROL LTP-II in the different operation/data processing modes.

LTP-II Operation Mode	Linear Variation Coefficient, g_1
SGB/CCP	$0.025324 \pm 6.4\times10^{-6}$ lines/mm^2
SGB/GMF	$0.025355 \pm 4.3\times10^{-6}$ lines/mm^2
PBI/CCP	$0.025370 \pm 5.0\times10^{-6}$ lines/mm^2
PBI/ SOPF	$0.025418 \pm 3.3\times10^{-6}$ lines/mm^2

Note that in all four modes of operation, the statistical errors are significantly smaller (by approximately two order of magnitude) than the variation of the results of fitting for g_1. This directly relates to the difference in the residual variation of the corresponding groove density distributions, shown in Figs. 8-11 and discussed above.

Finally, we present the results of fitting of the same measured density distributions with 3rd-order polynomial function – Tables 3 and 4. The corresponding residual (after subtraction of the trend described with the best-fit 3rd-order polynomial function) groove density variations are practically random.

Besides determining the low spatial frequency error of the grating, described with the parameters g_2 and g_3, such fitting is interesting from the point of view of estimation of the statistical errors for the higher order polynomial coefficients, achievable in the LTP-II measurement, discussed in this report.

Table 3: Specification of the LCLS grating groove density distribution and the results of the measurements performed at the ALS XROL with the LTP-II in the SGB arrangement and two different mode of calculation of the slope angle, centroid calculation positioning (CCP) and Gaussian maximum fitting (GMF). The residual (after subtraction of the best-fit 3rd order polynomial) groove density variations are shown in Figs. 8 and 9.

Parameter	Specification	XROL LTP-II in SGB/CCP mode	XROL LTP-II in SGB/GMF mode
g0 (l/mm)	300.0	$300.0 + (-0.00027 \pm 0.00022)$	$300.0 + (-0.00091 \pm 0.00014)$
g1 (l/mm^2)	0.0252	$0.0253238 \pm 6.4\times10^{-6}$	$0.0253668 \pm 4.1\times10^{-6}$
g2 (l/mm^3)	0	$-2.554\times10^{-7} \pm 4.97\times10^{-8}$	$-6.71\times10^{-8} \pm 3.21\times10^{-8}$
g3 (l/mm^4)	0	$1.034\times10^{-8} \pm 9.81\times10^{-10}$	$4.47\times10^{-9} \pm 6.33\times10^{-10}$

Table 4: Specification of the LCLS grating groove density distribution and the results of the measurements performed at the ALS XROL with the LTP-II in the PBI arrangement and using two different algorithms for calculation of the slope angle, centroid calculation positioning (CCP) and second-order-polynomial fitting (SOPF). The residual (after subtraction of the best-fit 3rd order polynomial) groove density variations are shown in Figs. 10 and 11.

Parameter	Specification	XROL LTP-II in PBI/CCP mode	XROL LTP-II in PBI/SOPF mode
g0 (l/mm)	300.0	300.0 + (0.0027 ± 0.00017)	300.0 + (-0.001992 ± 0.000113)
g1 (l/mm^2)	0.0252	0.0253700 ± 5.04×10^{-6}	0.0254184 ± 3.3×10^{-6}
g2 (l/mm^3)	0	-1.37×10^{-7} ± 3.9×10^{-8}	$+1.38\times10^{-7}$ ± 2.5×10^{-8}
g3 (l/mm^4)	0	2.50×10^{-9} ± 7.7×10^{-10}	8.73×10^{-10} ± 4.97×10^{-10}

Similar to the results in Table 2, the statistical errors for the fitting parameters of third-order polynomial are significantly (by approximately two order of magnitude) smaller than the variation of the best-fit parameters of fitting g_1, g_2, and g_3. This probably relates to the difference of random and systematic errors of the measurements. Therefore, currently, we can estimate the achievable accuracy of measurements of the corresponding parameters as

$$\begin{aligned} \delta g_1 &\approx 5\cdot10^{-5} \text{ lines/mm}^2, \\ \delta g_2 &\approx 2\cdot10^{-7} \text{ lines/mm}^3, \text{ and} \\ \delta g_3 &\approx 1\cdot10^{-8} \text{ lines/mm}^4. \end{aligned} \tag{9}$$

5. CONCLUSIONS

We have presented the results of the measurements of the groove density distribution of a VLS x-ray diffraction grating, fabricated for the LCLS. For the measurements, we have used our long trace profiler LTP-II in different operation and data processing modes. We have tested the single Gaussian beam, SGB, and the pencil beam interferometer, PBI, arrangement of the LTP-II. For each arrangement, we have used two data processing algorithms: with calculating the centroid position of the detected beam intensity distributions (the CCP fitting algorithm) and with determining the position of a characteristic features of the detected intensity distributions. These are the position of the maximum of the SGB image (the GMF fitting algorithm) and the position of the minimum of the PBI interference pattern (the SOPF fitting algorithm).

The major observation from the LTP-II measurements with the grating is the strong correlation between the LTP-II mode of operation and the residual (after subtraction of the best-fit 1st- or 3rd-order polynomial functions) groove density variation. The smaller residual variation corresponds to the operation modes the SGB/GMF and PBI/SOPF with lower spatial resolution [3,10].

However, from the presented data we can conclude that the difference of the tested LTP-II modes in the effective lateral resolution hardly explains the observed significant difference of the low-spatial-frequency variations of the residual groove density distributions, extracted from the same measurement data, but processed with different algorithms (compare Fig. 8 and Fig 9, and Fig. 10 and Fig. 11). The observed difference may also relate to a difference of the systematic errors of the LTP-II in the different operation/data processing modes, discussed first in Ref. [11] (see also Ref. [3]).

An indirect hint to the speculation about different systematic errors in the different modes of the LTP-II measurements can be seen in Fig. 12. Here, we present the residual slope variation of the grating surface measured in the zero-order diffraction arrangement with the LTP-II in SGB mode, with the recorded data processed in both CCP and GMF fitting routines. Because the surface of the substrate is flat, the slope variation is small, and correspondingly, the contribution of the LTP-II angular systematic error to the data in Fig. 12 is also small. Indeed, in the absence of the systematic error, the surface residual slope variations obtained are remarkably similar, in spite of the fact that the spatial resolution of the LTP-II in the different fittings is significantly different.

In Ref. [3], we investigate the dependence of the angular systematic error on the operation/data processing mode of the LTP-II using simulations with the optical model of the LTP under development [16].

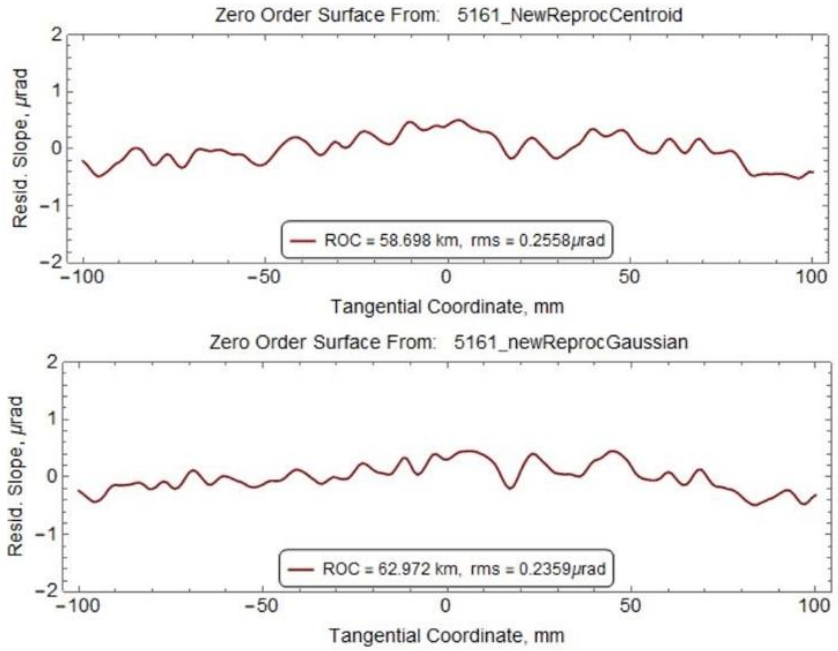

Figure 12: The residual (after subtraction of the best-fit linear trend) slope variation of the grating substrate surface as recorded by the LTP-II in the SGB/CCP (the tope plot) and SGB/GMF modes (the bottom plot).

In conclusion, we can use the observed variations of the parameters of the polynomial function, best-fitting the groove density distributions extracted from the measurement data, obtained with the LTP-II in different modes to estimate the current achievable accuracy of measurements of the corresponding parameters (note that the current version of the LTP-II is not capable to measure the g_0 parameter) as

$$\delta g_1 \approx 5\cdot 10^{-5} \text{ lines/mm}^2,\ \delta g_2 \approx 2\cdot 10^{-7} \text{ lines/mm}^3, \text{ and } \delta g_3 \approx 1\cdot 10^{-8} \text{ lines/mm}^4.$$

These estimations can be compared with the accuracy achieved in the ZYGO NewView-7300 microscope measurements with the 300-lines/mm VLS diffraction gratings, developed for the ALS MAESTRO beamline:

$$\delta g_0 \approx 1.5\cdot 10^{-2} \text{ lines/mm},\ \delta g_1 \approx 3\cdot 10^{-4} \text{ lines/mm}^2, \text{ and } \delta g_2 \approx 5\cdot 10^{-6} \text{ lines/mm}^3.$$

The results of these measurements are discussed in detail in Ref. [18]. Compared with the values in Refs [18], the accuracy of the microscope measurement, shown above, has been corrected by a factor of 3 in order to account the increase of the accuracy made possible after the recent upgrade of the microscope with a higher resolution camera.

ACKNOWLEDGEMENTS

The authors are very thankful to Daniele Cocco and the LCLS metrology group, and especially to May Ling Ng for very useful discussions.

The Advanced Light Source is supported by the Director, Office of Science, Office of Basic Energy Sciences, Material Science Division, of the U.S. Department of Energy under Contract No. DE-AC02-05CH11231 at Lawrence Berkeley National Laboratory.

Disclaimer

REFERENCES

[1] Kirschman , J. L., Smith, B. V., Domning, E. E., Irick, S. C., MacDowell, A. A., McKinney, W. R., Morrison, G. Y., Warwick, T., and Yashchuk, V. V., "Flat-Field Calibration of CCD Detector for Long Trace Profiler," Proc. SPIE 6704, 67040J (2007); doi: 10.1117/12.732618.

[2] Yashchuk, V. V., Artemiev, N. A., Lacey, I., McKinney, W. R., and Padmore, H. A., "Advanced environmental control as a key component in the development of ultra-high accuracy ex situ metrology for x-ray optics," Opt. Eng. 54(10), 104104/1-14 (2015); doi: 10.1117/1.OE.54.10.104104.

[3] Yashchuk, V. V., Lacey, I., Anderson, K., Dickert, J., Smith, B. V., and Takacs, P. Z., "Multifunctional light beam source for surface slope measuring long trace profilers" (This conference, paper No. 11492-3, Tracking No. OP20O-OP314-19).

[4] Cocco, D., Sostero, G., and Zangrando, M., "Technique for measuring the groove density of diffraction gratings using the long trace profiler," Rev. Sci. Instrum. 74(7), 3544-3548 (2003); https://doi.org/10.1063/1.1584080.

[5] Thomasset, M., Dvorak, J., Brochet, S., Dennetiere, D., and Polack, F., "Grating metrology for X-ray and V-UV synchrotron beamlines at SOLEIL," Rev. Sci. Instrum. 90(2), 021714 (2019); https://doi.org/10.1063/1.5055284.

[6] Siewert, F., Lammert, H., Reichardt, G., Hahn, U., Treusch, R., and Reininger, R., "Inspection of a spherical triple VLS-grating for self-seeding of FLASH at DESY," AIP Conf. Proc. 879, 667-670 (2007); https://doi.org/10.1063/1.2436150.

[7] Yashchuk, V. V., Lacey, I., and Smith, B. V., "First measurements of groove density distribution of x-ray VLS diffraction grating with the upgraded XROL LTP-II," LSBL Note LSBL-1348 (March 23, 2018).

[8] Chuang, Y.-D., Guo, J. H., "Specification of ruling and coating of diffraction gratings for X-ray emission spectrograph," Enginiring Specification," ALS, Berkeley (March 07, 2017).

[9] Polonska, K. S., Gevorkyan, G. S., and Yashchuk, V. V., "Surface slope deflectometer for characterization of diffraction gratings: Part 1: Estimation of the required accuracy of groove density measurements," LSBL Note LSBL-1310 (August 15, 2016 -March 10, 2017).

[10] Yashchuk, V. V., Lacey, I., Arnold, T., Paetzelt, H., Rochester, S., Siewert, F., and Takacs, P.Z., "Investigation on lateral resolution of surface slope profilers," Proc. SPIE 11109, 111090M (2019); doi: 10.1117/12.2539527.

[11] Centers, G., Smith, B. V., and Yashchuk, V. V., "New operational mode of the pencil beam interferometry based LTP," Proc. SPIE 9962, 996202/1-13 (2016); doi:10.1117/12.2238298.

[12] Nikitin, S. M., Gevorkyan, G. S., McKinney, W. R., I. Lacey, P. Z. Takacs, and V. V. Yashchuk, "New twist in the optical schematic of surface slope measuring long trace profiler," Proc. SPIE 10388, 103850I-1-17 (2017); doi: 10.1117/12.2274400.

[13] Yashchuk, V. V., Optimal Measurement Strategies for Effective Suppression of Drift Errors, Rev. Sci. Instrum. 80, 115101/1-10 (2009); doi: 10.1063/1.3249559.

[14] Lacey, I., Anderson, K., Centers, G. P., Geckeler, R. D. Gevorkyan, G. S., Just, A., Nicolot, T., Smith, B. V., and Yashchuk, V. V., "The ALS OSMS: Optical Surface Measuring System for high accuracy two-dimensional slope metrology with state-of-the-art x-ray mirrors," Proc. SPIE 10760, 1076002 (2018); https://doi.org/10.1117/12.2321347.

[15] Yashchuk, V. V., Lacey, I., Gevorkyan, G. S., McKinney, W. R., Smith, B. V., and Warwick, T., "Ex situ metrology of aspherical pre-shaped x-ray mirrors at the Advanced Light Source," Rev. Sci. Instrum. 90(2), 021711 (2019); doi: 10.1063/1.5057441.

[16] Takacs, P.Z., Lacey, I., and Yashchuk, V. V., "Raytracing the Long Trace Profiler" (This conference, paper No. 11492-2, Tracking No. OP20O-OP314-12).
[17] Ali, Z., Artemiev, N. A., Cummings, C. L., Domning, E. E., Kelez, N., McKinney, W. R., Merthe, D. J., Morrison, G. Y., Smith, B. V., and Yashchuk, V. V., "Automated suppression of errors in LTP-II slope measurements with x-ray optics," Proc. SPIE 8141, 81410O-1-15 (2011); http://dx.doi.org/10.1117/12.894061.
[18] Yashchuk, V. V., McKinney, W. R., and Artemiev, N. A., "Ex situ metrology of x-ray diffraction gratings," Nucl. Instr. and Meth. A 710, 59-66 (2013); http://dx.doi.org/10.1016/j.nima.2012.10.109.